Electrokinetic instabilities in thin microchannels

Brian D. Storey and Burt S. Tilley
Franklin W. Olin College of Engineering, Needham, Massachusetts 02492

Hao Lin and Juan G. Santiago
Department of Mechanical Engineering, Stanford University, Stanford, California 94305

(Received 26 May 2004; accepted 5 October 2004; published online 1 December 2004)

An important class of electrokinetic, microfluidic devices aims to pump and control electrolyte working liquids that have spatial gradients in conductivity. These high-gradient flows can become unstable under the application of a sufficiently strong electric field. In many of these designs, flow channels are thin in the direction orthogonal to the main flow and the conductivity gradient. Viscous stresses due to the presence of these walls introduce a stabilizing force that plays a major role in determining the overall instability. A thin channel model for fluid flow is developed and shown to provide good agreement with a complete three-dimensional model for channel aspect ratios $\lesssim 0.1$. © *2005 American Institute of Physics*. [DOI: 10.1063/1.1823911]

Instabilities in electrically driven microchannel flows with conductivity gradients have received recent attention in the literature[1–3] due to their relevance in micrototal analysis systems.[4–6] Melcher and co-workers developed much of the basic framework on these electrohydrodynamic instabilities in the 1960s–1980s (see Ref. 7 and references therein). Hoburg and Melcher first studied the basic conductivity gradient instability that is the focus of this work.[8] In recent work, three of us (B.D.S., H.L., J.G.S.) with Oddy and Chen have experimentally, analytically, and numerically investigated electrokinetic instabilities at the interface of two liquid streams in a microchannel subjected to an electric field perpendicular to the conductivity gradient.[1] In that work we demonstrated via three-dimensional (3D) linear analysis that the top and bottom walls of a shallow channel stabilized the flow with respect to two-dimensional (2D) predictions. Two of us (J.G.S., H.L.) together with Chen and Lele also showed that depth-averaged linearized governing equations could be used to analyze convective instabilities in microchannels.[2] Here we build upon this prior work and present a nonlinear model for electrokinetically driven flows in thin channels. We find good agreement when we compare our model to results obtained with 3D simulations.

The geometry of our study is provided by the experimental shallow channel described in detail in Ref. 1. The channel depth in the z direction, $2d$, is shallow compared to the channel width in the y direction, $2H$. The flow and imposed electric field E_o are along the channel length in the x direction. Initially, the conductivity is uniform in the z direction and varies in the y direction. Spontaneous charge separation at the walls of the channel form electric double layers (EDLs) with a thickness characterized by the Debye length.[9] Typical microchannel flows have an EDL of 10 nm or less while the channel dimensions are typically 10 μm or greater meaning that the liquid in the bulk may be modeled with slip velocity conditions prescribed at the walls.[9,10] In the thin channel configuration the instability generates a strong secondary flow predominantly in the x-y plane.

We start the analysis with the governing equations provided by Lin *et al.*[1] These equations already make use of the assumption that the charge density instantly relaxes compared to the rate of change of the conductivity.

$$0 = \nabla \cdot (\sigma \nabla \Phi), \tag{1}$$

$$\epsilon \nabla^2 \Phi = -\rho_E, \tag{2}$$

$$\nabla \cdot \mathbf{v} = 0, \tag{3}$$

$$\frac{D\sigma}{Dt} = D\nabla^2 \sigma, \tag{4}$$

$$\rho \frac{D\mathbf{v}}{Dt} = -\nabla P + \mu \nabla^2 \mathbf{v} - \rho_E \nabla \Phi, \tag{5}$$

where $\mathbf{v}$ is the velocity, σ is the conductivity, Φ is the electric potential, ρ_E is the charge density, ρ is the mass density, D is the diffusivity, ϵ is the permittivity, and μ is the viscosity.

To nondimensionalize the problem, we follow Ref. 1; only, we introduce two length scales into the problem. The scales used are $[x]=H$, $[y]=H$, $[z]=d$, $[u,v]=U_{ev}$, $[w]=U_{ev}\delta$, $[t]=H/U_{ev}$, $[\Phi]=E_o H$, $[\rho_E]=\epsilon E_o/H$, $[\sigma]=\sigma_o$, and $[P]=\epsilon E_o^2$, where the electroviscous velocity is $U_{ev}=\epsilon E_o^2 H\delta^2/\mu$ and the channel aspect ratio is $\delta=d/H$. This scaling yields the following equation set:

$$0 = \delta^2(\nabla_H \cdot \sigma \nabla_H \Phi) + (\sigma \Phi_z)_z, \tag{6}$$

$$-\delta^2 \rho_E = \Phi_{zz} + \delta^2 \nabla_H^2 \Phi, \tag{7}$$

$$0 = \nabla_H \cdot \mathbf{u} + w_z, \tag{8}$$

$$\delta^2 \mathrm{Ra} \frac{D\sigma}{Dt} = \sigma_{zz} + \delta^2 \nabla_H^2 \sigma, \tag{9}$$

$$\delta^2 \mathrm{Re} \frac{D\mathbf{u}}{Dt} = -\nabla_H P + \delta^2 \nabla_H^2 \mathbf{u} + \mathbf{u}_{zz} - \rho_E \nabla_H \Phi, \tag{10}$$

$$\delta^4 \mathrm{Re}\frac{Dw}{Dt} = -P_z + \delta^2(\delta^2\nabla_H^2 w + w_{zz}) - \rho_E \Phi_z, \tag{11}$$

where we use $\nabla_H \equiv (\partial_x, \partial_y)$ and $\mathbf{u} \equiv (u,v)$ for convenience. Subscript z denotes partial differentiation with respect to that direction. The Reynolds and electric Rayleigh numbers are, respectively, $\mathrm{Re} = \rho U_{ev} H/\mu$ and $\mathrm{Ra} = U_{ev} H/D$.[1,2] This scaling is appropriate for cases where the thickness of the diffusion layer between the regions of high and low conductivity is on the order of the width of the channel. The normal components of velocity, electric field, and conductivity gradient vanish at the walls. The liquid flow field is also bounded by a slip plane which excludes the EDLs of the system and at which the electroosmotic velocity is directly proportional to the local field[9,10]

$$\mathbf{v}\cdot\mathbf{t} = -\frac{1}{R_v}\zeta \boldsymbol{\nabla}\Phi\cdot\mathbf{t}, \tag{12}$$

where $1/R_v = \zeta_R H/E_o d^2$ is the ratio of electroosmotic velocity to electroviscous velocity.[2] We adopt the empirical correlations $\zeta(\sigma) = (\sigma/\sigma_R)^{-1/3}$ where σ_R is a reference conductivity at which the ζ-potential becomes $\zeta = \zeta_R$.[1,11]

We make the asymptotic assumption that all variables follow an expansion of the form $f = f_o + \delta^2 f_1 + \cdots$ where δ is a small parameter. The leading order terms in the conductivity equation (9) and the relaxation equation (6) are

$$(\sigma_o \Phi_{oz})_z = 0, \tag{13}$$

$$\sigma_{ozz} = 0. \tag{14}$$

The Neumann boundary conditions at $z = \pm 1$ for both variables require that $\sigma_o = \sigma_o(x,y,t)$ and $\Phi_o = \Phi_o(x,y,t)$. Proceeding to the first-order correction in the voltage potential Φ_1 and conductivity σ_1 and again applying Neumann conditions at $z = \pm 1$ yields the equations for σ_o, Φ_o, and ρ_{Eo}:

$$\rho_{Eo} = -\nabla_H^2 \Phi_o, \tag{15}$$

$$\boldsymbol{\nabla}_H\cdot(\sigma_o \nabla_H \Phi_o) = 0, \tag{16}$$

$$\mathrm{Ra}\left(\frac{\partial \sigma_o}{\partial t} + \overline{\mathbf{u}}_o\cdot\nabla_H \sigma_o\right) = \nabla_H^2 \sigma_o. \tag{17}$$

The z-momentum equation (11) at leading order is

$$P_{oz} = -\rho_{Eo}\Phi_{oz}. \tag{18}$$

Since Φ_o does not vary in z, we conclude that $P_o = P_o(x,y,t)$. The momentum equations in the x-y plane to leading order become

$$\mathbf{u}_{ozz} = \nabla_H P_o + \rho_{Eo}\nabla_H \Phi_o. \tag{19}$$

Since the right-hand side is not a function of z we can integrate to obtain the velocity as a function of z and the depth-averaged velocity $\overline{\mathbf{u}}$ as

$$\mathbf{u}_o = \frac{z^2-1}{2}[\nabla_H P_o + \rho_{Eo}\nabla_H \Phi_o] - \frac{\zeta \nabla_H \Phi_o}{R_v}, \tag{20}$$

$$\overline{\mathbf{u}}_o = \frac{-1}{3}[\nabla_H P_o + \rho_{Eo}\boldsymbol{\nabla}_H \Phi_o] - \frac{\zeta \nabla_H \Phi_o}{R_v}. \tag{21}$$

From continuity we can solve for $w(z)$ and show that $\overline{w} = 0$, which allows us to obtain the pressure in terms of the voltage potential,

$$\nabla_H^2 P_o = \nabla_H\cdot\left(\frac{3\zeta\nabla_H\Phi_o}{R_v} - \rho_{Eo}\nabla_H\Phi_o\right). \tag{22}$$

Equations (15)–(17), (21), and (22) represent a complete set of nonlinear, depth-averaged, and two-dimensional equations for application toward thin channels.

We can analyze the instability in a periodic channel by linearizing the equations about a base state solution using normal modes; $f(x,y,t) = f_b(y) + \hat{f}(y)e^{ikx+st}$. For our study, the steady base state consists of an initial conductivity gradient $\sigma_b(y)$ and an imposed uniform electric field in the x direction. These conditions generate a nonzero electroosmotic u velocity gradient $u_b = \zeta[\sigma_b(y)]/R_v$. The linearization results in the following set of equations for the disturbances $\hat{P}$, $\hat{\Phi}$, and $\hat{\sigma}$:

$$ik\hat{\sigma} = \sigma_b \nabla_H^2 \hat{\Phi} + \frac{d\sigma_b}{dy}\frac{d\hat{\Phi}}{dy}, \tag{23}$$

$$\nabla_H^2 \hat{P} = \frac{3}{R_v}\left(ik\frac{d\zeta}{d\sigma}\hat{\sigma} - \frac{d\zeta}{dy}\frac{d\hat{\Phi}}{dy}\right) - \left(\frac{3\zeta}{R_v} + ik\right)\nabla_H^2\hat{\Phi}, \tag{24}$$

$$s\hat{\sigma} = \frac{\nabla_H^2\hat{\sigma}}{\mathrm{Ra}} - \frac{ik\zeta\hat{\sigma}}{R_v} + \left(\frac{1}{3}\frac{d\hat{P}}{dy} + \frac{\zeta}{R_v}\frac{d\hat{\Phi}}{dy}\right)\frac{d\sigma_b}{dy}. \tag{25}$$

Neumann boundary conditions apply for each of the variables where the pressure boundary condition corresponds to the zero normal velocity condition.

To validate the model, we compare the flow fields computed from Eqs. (23)–(25) to the three-dimensional solution. Details of the three-dimensional simulation are discussed in Ref. 1. In Fig. 1 we show a representative snapshot of the flow field in a cross-stream (y-z) plane as computed from the linearized thin channel model and the three-dimensional model, respectively. Figure 1 shows solutions where linearization about the base state is valid. Results show excellent agreement in the shape and magnitude of the flow field in this and many other cases. The most striking difference is seen at the upper and lower boundaries for the $\hat{u}$ velocity. The depth-averaged formulation cannot prescribe the boundary conditions on $\hat{u}$ at $y = \pm 1$ boundaries, which contrasts with the electroosmotic boundary condition in the 3D formulation. This difference in the boundary condition is expected due to the overall reduction of the order of the equations in making a 2D approximation of a 3D flow. A boundary-layer approach was implemented to show that this effect is higher order in δ and does not appreciably influence the interior flow. Our numerical simulation confirms this result.

A representative stability diagram for the flow in a 10:1 aspect ratio channel is shown in Fig. 2. The results are shown in dimensional form using the physical parameters provided in Ref. 1. The thin channel model provides good agreement

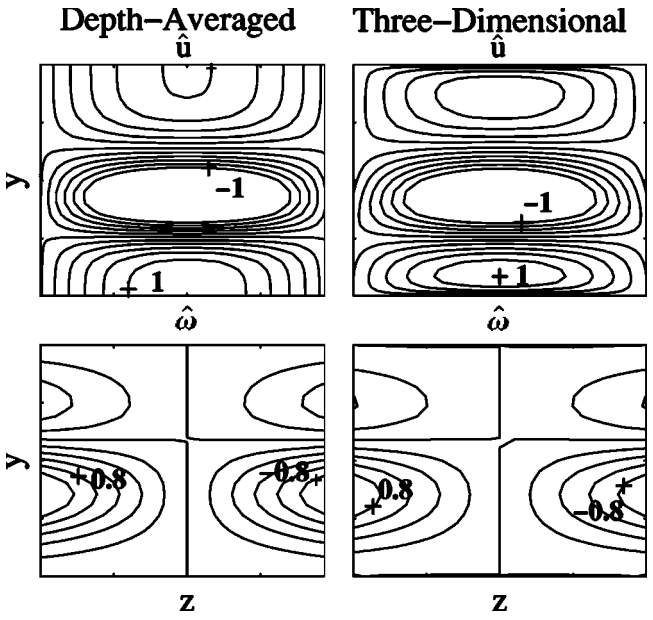

FIG. 1. Representative snapshot comparison of the flow field in the *y*-*z* plane computed from the depth-averaged (left) and the three-dimensional model (right). Contours are provided for the *x* component of the perturbation velocities $\hat{u}$ and the *x* vorticity $\hat{\omega}_x$. Contour levels are the same on the left and right, are normalized by the maximum in the 3D field, and have contour increments of 0.2. The channel aspect ratio is 10:1.

at low wavenumbers when compared to the complete 3D formulation.[1] We see good agreement for $k<2$ and find that the depth-averaged model loses accuracy as the wavenumber increases. We have confirmed that at higher aspect ratios, the model provides accurate results at higher wavenumbers suggesting the model can only capture motions where $k\delta$ is small. Despite this shortcoming, the current 2D model provides more realistic physics and more accurate results than a 2D analysis that does not account for the thin geometry.[1]

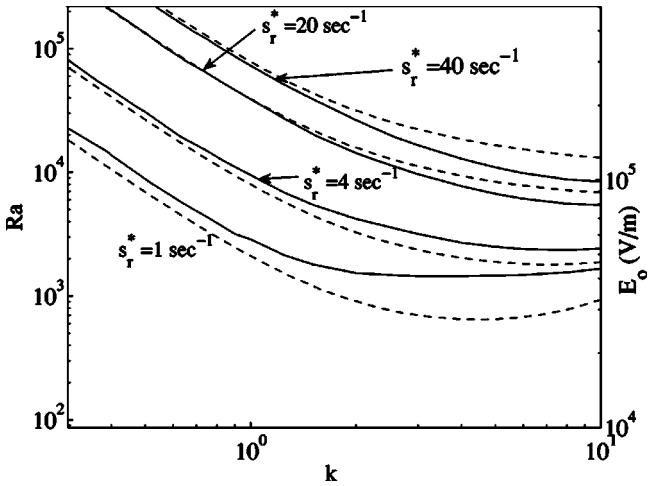

FIG. 2. Contours of the dimensional real growth rate for a channel with $\delta=0.1$. The solid lines are from the linearized three-dimensional equations and the dotted lines are from the depth-averaged model. Conditions are the same as in Ref. 1 and the solid curves correspond to the data presented in Fig. 10 of Ref. 1; however, note that the scaling for Ra has changed to incorporate the thin channel.

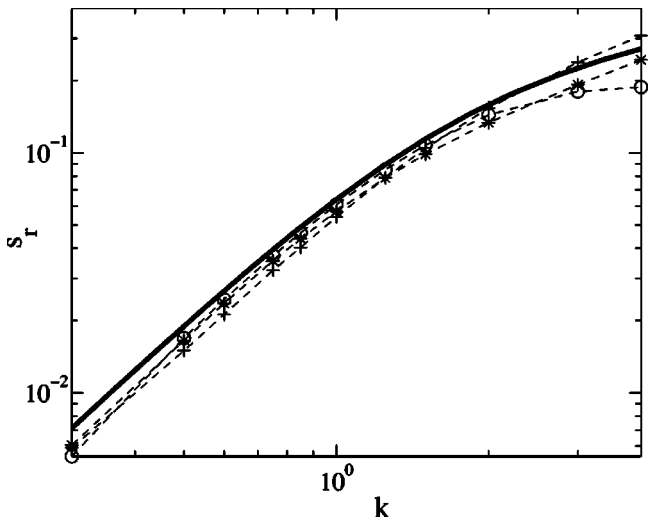

FIG. 3. Real growth rate as a function of wavenumber from Eq. (26) (thick solid line) compared to results from the complete 3D model. The data show results from channels with different aspect ratios, 1:10 (+), 1:20 (∗), and 1:40 (○). For the 3D simulations we used Ra=10 000 and $R_v=20$.

The stability behavior can be interpreted more concisely if we consider the limit where the diffusion of conductivity is slow compared to the convective motions (Ra=∞) and the electroviscous velocity dominates over electroosmotic velocity ($R_v=\infty$). Equations (23)–(25) can be reduced to a single equation with no free parameters, only the assumed initial conductivity profile σ_b,

$$s\left[\sigma_b\nabla_H^2+\frac{d\sigma_b}{dy}\frac{d}{dy}\right]\hat{\Phi}=\frac{k^2}{3}\frac{d\sigma_b}{dy}\frac{d\hat{\Phi}}{dy}. \tag{26}$$

The solution to Eq. (26) (for our assumed conductivity profile) is shown as the thick solid line in Fig. 3. On the same figure we also compare results from the full three-dimensional simulation at conditions where Ra and R_v are both large. The 3D results collapse on this single curve at small wavenumbers. The electroviscous time scale is therefore an excellent indicator in determining the characteristic growth rate of the instability (see also Fig. 8 in Ref. 1).

We can now turn to the solution of Eqs. (23)–(25) to complete our understanding. In Fig. 4(a) we show contours of the real part of the growth rate as a function of wavenumber and R_v in the infinite Ra limit. Above $R_v=10$ the electroosmotic effect has little influence on the overall stability picture; this result agrees with that of Ref. 2. In Fig. 4(b) we show contours of the real part of the growth rate as a function of wavenumber and Ra in the $R_v=\infty$ limit. For Rayleigh numbers above 10 000, Fig. 3 is an accurate model of the flow.

Diffusion alters the base conductivity state as a function of time, an effect not captured in Eqs. (23)–(25). Therefore, the results in Fig. 4(b) are not valid for cases where the time scale for instability is long compared to the time for diffusion across the width (*y* direction) of the channel. For such cases perturbations cannot grow quickly enough to overcome the diffusion of the base state. This ratio of time scales in dimensionless form is s_rRa and we use $s_r\text{Ra}>50$ as a criterion to

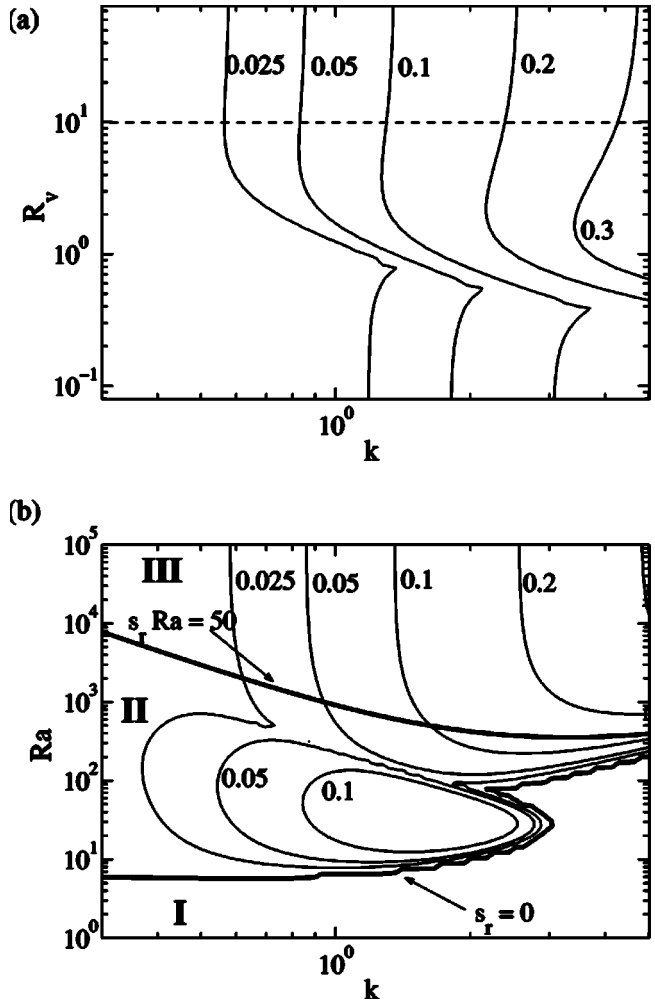

FIG. 4. (a) Contours of the real growth rate as a function of wavenumber and R_v when Ra$=\infty$. (b) Contours of the real growth rate as a function of wavenumber and Ra when $R_v=\infty$. We find that above $R_v=10$ and Ra $=10\,000$ Fig. 3 is a valid picture of the stability behavior. Contours in both figures are generated from Eqs. (23)–(25). The three regimes I, II, and III are denoted in part (b) (see text).

determine if the diffusing base state is relevant, where s_r denotes the real part of the growth rate. The criterion is somewhat arbitrary and there is not a clearly defined regime boundary. There are three important regimes: (I) negative growth rates where mixing of the base state occurs by diffusion alone, (II) marginally unstable, low magnitude positive growth rates where diffusion of the base state dominates the growth of the perturbation, and (III) the regime where growth rates are positive and large compared to diffusion of the base state, and rapid mixing occurs due to the instability. Further discussion of the unsteady, diffusive base state is found in Ref. 1.

In conclusion, we have shown the depth-averaged model for electrokinetic flows in thin channels provides good agreement when compared to three-dimensional simulations. The stability analysis can be collapsed to a single equation in the limit of high electric fields and negligible electroosmotic flow which simplifies analysis and understanding. We note that the model can only reliably capture motions where $k\delta$ is small, while 3D simulations and experiments indicate high wavenumber disturbances are often prominent. However, the underlying behavior of the instability is well captured by our model and the predictions are valid as long as the flow features remain "thin." Higher order corrections or nonlinear three-dimensional simulations are needed to fully model higher wavenumber flow.

[1] H. Lin, B. D. Storey, M. H. Oddy, C.-H. Chen, and J. G. Santiago, "Instability of electrokinetic microchannel flows with conductivity gradients," Phys. Fluids **16**, 1922 (2004).
[2] C.-H. Chen, H. Lin, S. J. Lele, and J. G. Santiago, "Convective and absolute electrokinetic instability with conductivity gradients," J. Fluid Mech. (in press).
[3] J. C. Baygents and F. Baldessari, "Electrohydrodynamic instability in a thin fluid layer with an electrical conductivity gradient," Phys. Fluids **10**, 301 (1998).
[4] A. Manz, N. Graber, and H. Widmer, "Miniaturized total chemical analysis systems: A novel concept for chemical sensing," Sens. Actuators B **1**, 244 (1990).
[5] A. van den Berg and T. S. J. Lammerink, "Micro total analysis systems: Microfluidic aspects, integration concept," Top. Curr. Chem. **194**, 21 (1998).
[6] P. A. Auroux, D. Iossifidis, D. R. Reyes, and A. Manz, "Micro total analysis systems. 2. Analytical standard operations and applications," Anal. Chem. **74**, 2637 (2002).
[7] J. R. Melcher, *Continuum Electromechanics* (MIT Press, Cambridge, 1981).
[8] J. F. Hoburg and J. R. Melcher, "Internal electrohydrodynamic instability and mixing of fluids with orthogonal field and conductivity gradients," J. Fluid Mech. **73**, 333 (1976).
[9] R. Probstein, *Physicochemical Hydrodynamics* (Wiley, New York, 1994).
[10] J. G. Santiago, "Electroosmotic flows in microchannels with finite inertia and pressure forces," Anal. Chem. **73**, 2353 (2001).
[11] S. Yao and J. G. Santiago, "Porous glass electroosmotic pumps: Theory," J. Colloid Interface Sci. **268**, 133 (2003).